Applied Physics Letters

Tunable surface acoustic waves on strain-engineered relaxor $K_{0.7}Na_{0.3}NbO_3$ thin films

Cite as: Appl. Phys. Lett. **116**, 052902 (2020); https://doi.org/10.1063/1.5140259
Submitted: 26 November 2019 . Accepted: 24 January 2020 . Published Online: 06 February 2020

Sijia Liang, D. Pfützenreuter, D. Finck, L. von Helden, J. Schwarzkopf, and R. Wördenweber

Applied Physics Letters ARTICLE scitation.org/journal/apl

Tunable surface acoustic waves on strain-engineered relaxor $K_{0.7}Na_{0.3}NbO_3$ thin films

Cite as: Appl. Phys. Lett. **116**, 052902 (2020); doi: 10.1063/1.5140259
Submitted: 26 November 2019 · Accepted: 24 January 2020 ·
Published Online: 6 February 2020

Sijia Liang,[1,a)] D. Pfützenreuter,[2] D. Finck,[1] L. von Helden,[2] J. Schwarzkopf,[2] and R. Wördenweber[1]

AFFILIATIONS

[1]Institute of Complex Systems–Bioelectronics (ICS-8), Forschungszentrum Jülich, 52425 Jülich, Germany
[2]Leibniz Institute for Crystal Growth (IKZ), 12489 Berlin, Germany

[a)]Author to whom correspondence should be addressed: si.liang@fz-juelich.de

ABSTRACT

In this work, we demonstrate the electronic tunability of surface acoustic waves (SAWs) in epitaxially strained relaxor-type ferroelectric thin films. Epitaxial $K_{0.7}Na_{0.3}NbO_3$ thin films of typically 30 nm in thickness are grown via pulsed laser deposition on (110)-oriented $TbScO_3$. A partial plastic lattice relaxation of the epitaxial strain in these samples leads to a relaxor-type ferroelectricity of these films, which strongly affects the SAW properties. Without electronic bias, only tiny SAW signals of ∼0.2 dB can be detected at room temperature, which can be boosted up to ∼4 dB by a static voltage bias added to the high frequency driving current of the SAW transducers. Upon field cooling below the freezing temperature of polar nanoregions (PNRs), this strong SAW signal can be preserved and is even enhanced due to a release of the electronically fixed PNRs if the bias is removed. In contrast, at elevated temperatures, a reversible switching of the SAW signal is possible. The switching shows relaxation dynamics that are typical for relaxor ferroelectrics. The relaxation time τ decreases exponentially from several hours at freezing temperature to a few seconds (<5 s) at room temperature.

As surface acoustic wave (SAW) devices are presently widely used in communications nowadays, signal processing, and transducers, actuators, and sensor technologies, novel concepts for innovative applications ranging from highly sensitive and selective biosensors, microfluidics, and microactuators to complex lab-on-a-chip devices are increasingly becoming the focus of research on piezoelectric materials and SAW devices.[1–7] The main aims of this reinforcement of research activities are as follows: (i) the miniaturization and integration of SAW devices in complex systems, (ii) the replacement of $PbZr_{1-x}Ti_xO_3$-based ceramics,[8] and (iii) the search for novel functionalities (for example, the tunability of SAWs) of piezoelectric materials that could broaden the range of applications.[9–12] An appropriate solution would be to develop thin-film piezoelectric components with suitable properties. In previous work, we demonstrated the ability to tailor the properties of $(K,Na)NbO_3$ via epitaxial strain and thus generate strong SAWs in extremely thin films.[13]

In this work, we demonstrate that in relaxor-type $(K,Na)NbO_3$ thin films, SAW signals can be tuned and even switched on and off via a DC bias field. The strain-engineered $(K,Na)NbO_3$ films are partially relaxed and therefore show a broad and frequency-dispersive phase transition, which is a clear indication of relaxor-type ferroelectrics. The resulting SAW signal depends strongly on the orientation and mobility of the polar nanoregions (PNRs) of the relaxor state, which can be electronically manipulated.

$K_{0.7}Na_{0.3}NbO_3$ (KNN) films of 25–30 nm in thickness are deposited via pulsed laser deposition (PLD) onto (110)-oriented single crystalline $TbScO_3$ substrates using the following deposition parameters: a substrate temperature of 600 °C, an O_2 pressure of 0.3 mbar, a laser energy of 2.0 J/cm^2, a laser pulse frequency of 5 Hz, and a growth rate of 0.125 nm/pulse. For the electronic characterization of the films, interdigitated electrodes (IDEs) and transducers (IDTs) are fabricated using electron-beam lithography and the lift-off technique. The structures and parameters of IDEs and IDTs are the same as in our previous work.[13,14] They consist of a 5 nm thick Ti adhesion layer and a 45 nm thick Pt layer. The IDEs for the investigation of the dielectric properties of the KNN layer have 32 finger pairs with a width of 10 μm, a gap size of 5 μm, and an effective length of 700 μm, whereas the IDTs for SAW experiments consist of 4 finger pairs with 3 μm width and gap size, yielding a SAW wavelength of $\lambda = 12$ μm, an effective finger length of 500 μm, and a propagation distance (center-to-center distance between the generator and the analyzer) of $L = 500$ μm (see also the inset of Fig. 2).

X-ray reciprocal space maps (RSM) confirm the epitaxial growth of our KNN films, while at the same time, they indicate an onset of

plastic lattice relaxation of the strained films [Figs. 1(a) and 1(b)]. The maxima of the $q_{\parallel}$ positions of the KNN reflections coincide with the substrate reflections $(620)_{TSO}$ ($q_{\parallel} = 3.1733\ \text{Å}^{-1}$) and $(444)_{TSO}$ ($q_{\parallel} = 3.1745\ \text{Å}^{-1}$). However, both the absence of satellite patterns (indicative of a regular arrangement of domains[15]) and especially the broadness of the KNN layer reflection and its distortion in the direction of unstrained KNN are clear indications of a plastic relaxation of the strained KNN layer structure.

Usually, epitaxially strained films exhibit relaxor-type ferroelectric behavior.[16] This is even more likely for strained films showing plastic strain relaxation. The relaxors possess peculiar features that are correlated with the formation of polar nanoregions (PNRs). At high temperatures, relaxors exist in a non-polar paraelectric phase, which is similar to the paraelectric phase of ordinary ferroelectrics. Upon cooling, they transition into an ergodic relaxor state, in which polar regions are formed on the nm scale with a random orientation of dipole moment. Since relaxor-type behavior can strongly affect the ferroelectric properties, we first analyze the temperature and frequency dependence of the KNN film and demonstrate its textbook relaxor behavior.

Figure 1(c) shows the temperature dependence of the permittivity at the vicinity of the ferroelectric–ferroelectric transition from the monoclinic M_C to the orthorhombic c-phase[17] measured at different frequencies.

First, the broadness of the transition peak can be scaled according to the empirical Lorentz relation[18] $\varepsilon'_{max}/\varepsilon' = 1 + (T - T_{max})^{\gamma}/2\sigma^2$ for $T > T_{max}$, where ε'_{max} is the maximum permittivity at T_{max}, γ is the degree of dielectric relaxation, and σ is the degree of diffuseness of the phase transition. A sharp transition peak near $\gamma = 1$ indicates a conventional ferroelectric behavior, whereas the relaxor-type phase transition is usually characterized by a broad peak with γ ranging from 1.5 to 2. Our KNN film shows a broad peak with $\gamma \approx 1.9$ [see Fig. 1(e)].

Second, not only the frequency dispersion of the permittivity but also the frequency dependence of the temperature T_{max} is a clear indication of a relaxor-type ferroelectric behavior. The frequency dependence of T_{max} [marked in Fig. 1(c)] of a relaxor typically obeys the empirical Vogel–Fulcher law[19,20] $f = f_0 \exp[-E_a/k_B(T_{max} - T_{VF})]$, with activation energy E_a, Vogel–Fulcher freezing temperature T_{VF}, attempt frequency f_0, and Boltzmann constant k_B. By choosing a reasonable attempt frequency f_0 (typically in the range of 1–4 THz[21,22]), we can extract $E_a \approx (113 \pm 9)$ meV and $T_{VF} \approx (211 \pm 26)$ K for our KNN film from the resulting Vogel–Fulcher fit [Fig. 1(d)]. The former describes the energy needed for the reorientation of the PNRs' polarization, while the latter characterizes the temperature below which the PNRs start to freeze, i.e., become immobile.

We therefore conclude that our PLD-prepared KNN films are textbook examples of relaxor-type ferroelectrics.

Figure 2 summarizes SAW data obtained at room temperature for a 25 nm-thick KNN film. A first complete frequency scan of the response of the IDTs oriented along the $[1\bar{1}0]_{TSO}$ direction shows a disappointingly small signal. As shown in previous work,[13] due to the thinness of the film and the design of the IDTs, only odd harmonic excitations are visible and the largest SAW signal is expected for the third harmonic at a center frequency of $f_3 = 828.8$ MHz. However, in these samples, the signal is hardly measurable for the first harmonic and very small for the third harmonic [e.g., $\Delta S_{21} \approx 0.2$ dB in Fig. 2(a)].

This situation changes significantly with the application of a DC bias. The amplitude of the SAW Fraunhofer pattern at the odd harmonics, which is attributed to the interference between acoustic and electromagnetic waves at the output IDTs,[23] is greatly boosted by the DC field. As shown in Fig. 2(b), $\Delta S_{21}(f_3)$ increases from ~0.2 dB for zero-field to ~4 dB at a DC bias of 20 V. The latter value is comparable to results obtained without bias for metal organic chemical vapor deposition (MOCVD)-grown KNN films with comparable thickness and stoichiometry but better crystallinity.[13]

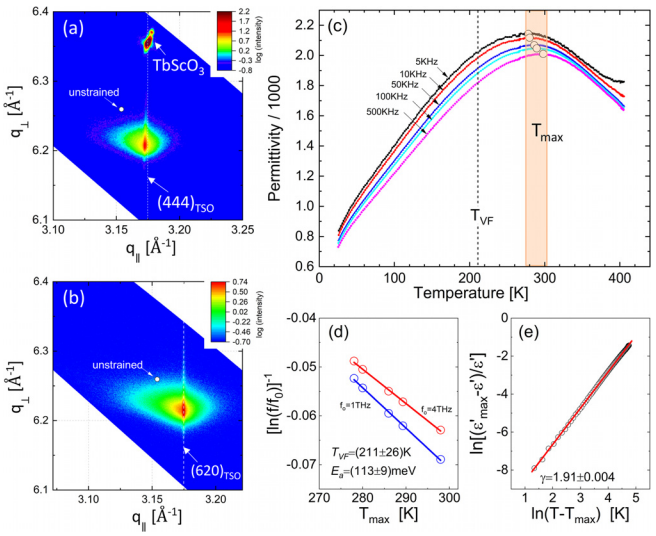

FIG. 1. X-ray reciprocal space maps (RSMs) in the vicinity of the (a) (444) and (b) (620) Bragg reflections of the $TbScO_3$ substrate, (c) temperature dependence of the real part of the dielectric permittivity for a 25 nm-thick $K_{0.7}Na_{0.3}NbO_3$ film on (110) $TbScO_3$ at different frequencies, (d) Vogel–Fulcher fit (solid line) using a reasonable range for the attempt frequency (1–4 THz), and (e) Lorentz fit (solid line) of the permittivity measured at 100 kHz. The dashed white lines and white dots in (a) and (b) mark the $q_{\parallel}$ position of $TbScO_3$ and the expected position of unstrained KNN, while the reddish shaded area in (c) marks the temperature regime of maximum permittivity.

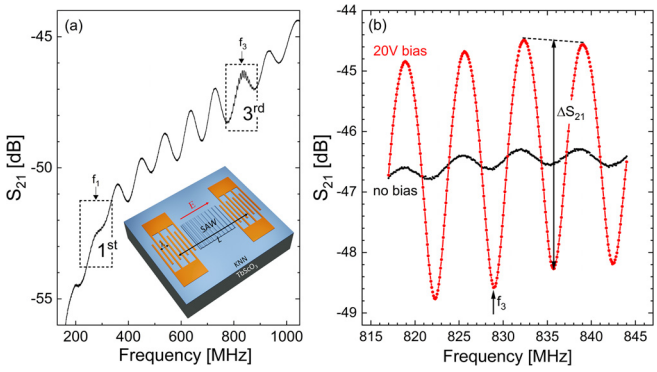

FIG. 2. Frequency dependence of the transmission signal of a SAW structure (inset) with IDTs with a periodicity $\lambda = 12\ \mu$m and a distance $L = 500\ \mu$m on a 25 nm-thick $K_{0.7}Na_{0.3}NbO_3$ film on (110) $TbScO_3$ measured along the $[1\bar{1}0]_{TSO}$ direction at room temperature. (a) shows the signal including the first (fundamental) and third harmonics for zero DC bias, whereas (b) provides a comparison of the zero bias and 20 V-bias signal at the third harmonic. The resulting SAW signal is characterized by the analysis of ΔS_{21} as indicated in (b).

Since the impact of the DC bias on the SAW signal might be attributed to the relaxor-type behavior of the KNN film, especially the arrangement and alignment of the PNRs, we examined the bias dependence of the SAW signal as well as its temperature dependence and relaxation behavior in more detail.

DC-bias dependence: Fig. 3 shows the DC-bias dependence of the SAW signal. We analyzed the electric field dependence of the maximum amplitude $\Delta S_{21}(f_3)$ by modifying the bias incrementally by ± 2 V (i.e., ± 4 V/mm) between -20 and 20 V starting at zero field. The DC field and SAWs are oriented in the $[1\bar{1}0]_{TSO}$ direction. The sample shows a butterfly-type tunability of the SAW signal.

(i) Generally, the SAW signal increases with the DC field for positive and negative biases. This increase seems to level off for a large field. Furthermore, a small asymmetry can be observed (i.e., the signal is larger for a positive field).

(ii) The bias dependence shows slight hysteretic behavior although all data points were recorded after a long stabilization (~20 min) at a given DC field.

The schematics in Fig. 3 illustrate the mechanism of the tunability of SAWs, which is believed to be related to the reorientation of the PNRs under the DC field. At a low DC field [inset (a)], the PNRs are randomly distributed in the matrix, and the disordered polarization state dramatically attenuates the generation and propagation of SAWs, resulting in a very weak SAW signal. Meanwhile, at a high DC field, the PNRs become oriented (or better oriented) by the E-field, inducing an ordered polarization state, which facilitates the generation and propagation of SAWs and thus a strong SAW signal.

Temperature dependence: Fig. 4 shows the temperature dependence of the SAW signal for the 25 nm-thick KNN film. Starting in the orthorhombic c-phase ($T \gg T_{max}$), no SAW signal can be detected without DC bias. An SAW signal only becomes visible after the DC bias is switched on (here, 40 V/mm at ~380 K). In terms of our explanation, this indicates that there are still a few PNRs at this temperature and that the polarization vectors of the normally randomly distributed and highly mobile PNRs will be oriented by the DC field, resulting in

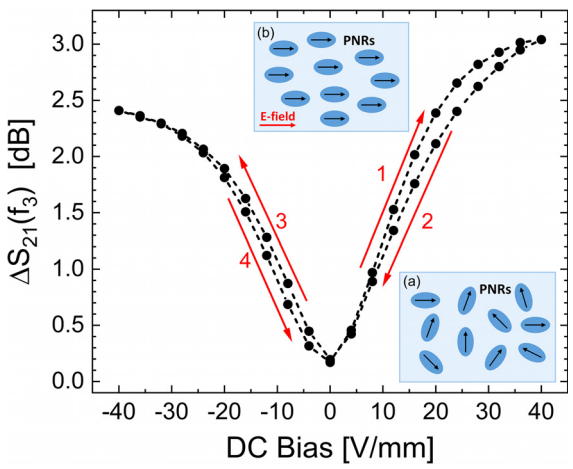

FIG. 3. DC-bias dependence of the SAW intensity for a 25 nm-thick $K_{0.7}Na_{0.3}NbO_3$ film on (110) $TbScO_3$ at room temperature. The red arrows reveal the sequence of applying the DC field; the dashed lines act as a visual guide.

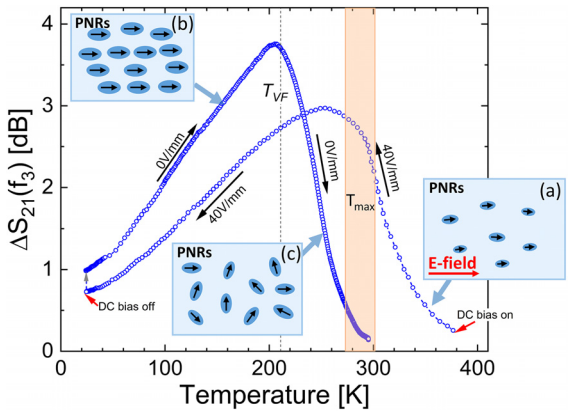

FIG. 4. Temperature dependence of SAW intensity for a 25 nm-thick $K_{0.7}Na_{0.3}NbO_3$ film on (110) $TbScO_3$. First, the sample is cooled from 400 K to 20 K with a DC bias of 40 V/mm, then the DC E-field is removed at the minimum temperature of ~20 K, and finally, the sample is heated up to room temperature again. The schematics illustrate the evolution of the PNR orientation for different states.

an ordered state [see inset (a) of Fig. 4] and a detectable SAW signal (e.g., ~0.2 dB at 380 K). Upon cooling, the size and amount of PNRs, and thus the SAW signal, increase.[24] At 253.6 K, slightly below the phase-transition temperature, the SAW signal reaches a first maximum of 2.97 dB. At even lower temperatures, the PNRs start to freeze, i.e., they become immobile. As a result of the reduced mobility of the PNRs, the SAW signal strength decreases. At the lowest temperature (here, ~20 K), we remove the DC bias. This removal of the field leads to a sudden increase in the SAW signal. At this temperature clearly below T_{VF}, it is expected that the ordered state of PNRs is preserved. However, tiny rearrangements of the PNRs might still be possible. By removing the restriction imposed by the DC field on the oriented PNRs, these small changes might be responsible for the significant increase in the SAW signal. We will see this *release mechanism* again in Fig. 5.

Upon heating, now without the DC field, the SAW intensity increases due to the increasing mobility of the PNRs. It reaches a maximum at approximately T_{VF} [$\Delta S_{21}(f_3) \approx 3.8$ dB]. In the temperature regime below T_{VF}, the SAW intensity is significantly higher than during cooling with the DC bias. This again can be attributed to the above-described release mechanism. Above the freezing temperature T_{VF}, the PNRs are no longer immobile, and the thermal motion leads to an order-disorder transition for the relaxor [inset (c) of Fig. 4]. As a consequence, the SAW intensity drops precipitously and can no longer be detected above room temperature.

Relaxation behavior: Finally, we investigated the dynamics of the bias release and relaxation of the PNRs. For this purpose, the sample is first heated to approximately 380 K (c-phase) and then cooled to a given temperature while applying a DC bias of 40 V/mm. After stabilizing at a given temperature, the bias is removed and the SAW signal is recorded for 1 h. Figure 5 shows the resulting development of the SAW signal for different temperatures. Generally, we observe (i) an initial sudden and significant increase in the signal (first data point recorded after ~5 s), (ii) followed by a more gentle increase toward (iii) a maximum in ΔS_{21} (at time t_{peak}), and (iv) henceforth a decrease in the SAW signal. The dynamics of the process strongly depend on

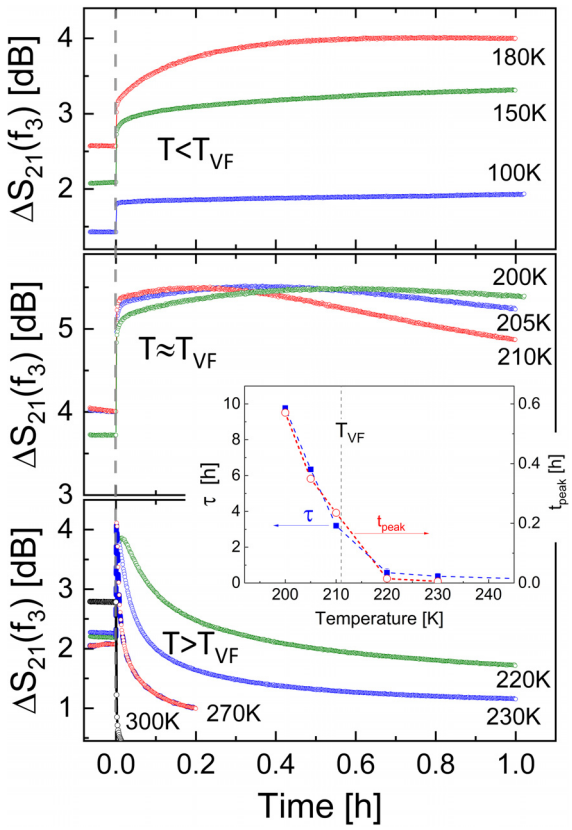

FIG. 5. Time dependence of the SAW signal after removing the DC bias (40 V/mm) at t = 0 for different temperatures for $T < T_{VF}$, $T \approx T_{VF}$, and $T > T_{VF}$. Prior to each experiment, the sample was heated to an elevated temperature (380 K) and subsequently cooled to a given temperature with an applied DC bias. The inset shows the temperature dependence of the relaxation time τ, which describes the exponential decay of the signal after the release of the electric field.

the temperature. At low temperatures ($T \ll T_{VF}$), we do not reach the maximum in ΔS_{21} within the measuring time. At T_{VF}, the maximum is reached after $t_{peak} \approx 0.2$ h, whereas for 220 K and 270 K, the peak is observed at ~1 min and ~5 s, respectively. The subsequent decrease in signal strength behaves similarly. It starts gently at low temperatures and becomes more rapid as the temperature increases.

Specifically, at higher temperatures (see curves for $T > T_{VF}$ in Fig. 5), a typical relaxation behavior toward a finite value can be observed. An exponential fit of this part of the curve (for $t > t_{peak}$) provides a characteristic relaxation time τ of the relaxation process. The inset of Fig. 5 shows the temperature dependence of τ and t_{peak}. First, the relaxation time seems to be correlated with the freezing process of the PNRs. Far above the freezing temperature T_{VF}, it is extremely small (e.g., $\tau(270\,K) \approx 150$ s); close to T_{VF}, it rapidly (exponentially) increases (e.g., from $\tau(230\,K) \approx 22$ min to $\tau(200\,K) \approx 9.8$ h); and finally, below T_{VF}, the relaxation is no longer recorded. Second, t_{peak} shows a very similar temperature dependence, i.e., it increases rapidly upon approaching the freezing temperature. Therefore, we conclude that, except for the initial jump in ΔS_{21} (release mechanism), the further development of the SAW signal is caused by one and the same relaxation mechanism, which first ($t < t_{peak}$) leads to an increase and then ($t > t_{peak}$) to a decrease in ΔS_{21}. The temperature dependence of τ and t_{peak} indicates that this mechanism is based on the relaxation of PNRs, i.e., a consequence of the relaxor-type behavior of the film.

In conclusion, our PLD-grown KNN films on (110) $TbScO_3$ show very promising SAW properties. The SAW response of the only ~30 nm-thick films is quite strong compared to other piezoelectric film systems,[25–28] which are typically several μm thick. Moreover, in contrast to comparable MOCVD-grown stained KNN films with a more perfect crystallinity,[13] the plastic relaxation in these samples leads to an electronic tunability of the SAW signal, which is ascribed to the relaxor-type ferroelectricity of these films. Without electronic bias, only tiny signals (~0.2 dB) can be detected. However, a DC bias of just 40 V/mm can boost the signal up to ~4 dB, which is even comparable to bulk SAW devices based on other relaxor systems such as KNN-$SrTiO_3$ and PMN-PT.[29,30] At temperatures below the freezing temperature for PNR motion, this strong SAW signal can be preserved and can even be enhanced due to a release of the electronically fixed PNR. At elevated temperatures, in contrast, a reversible switching of the SAW signal is possible. The switching shows relaxation dynamics that are typical for relaxor ferroelectrics. The relaxation time τ decreases exponentially from several hours at the freezing temperature to a number of seconds at room temperature. The use of epitaxially strained relaxor-type ferroelectric films could represent an option for the development of electronically tunable SAW devices.

The authors would like to thank A. Offenhäusser, R. Kutzner, S. Trellenkamp, U. Breuer, S. Ganschow, the Helmholtz Nanoelectronic Facility (HNF), and the Working Group Oxides and Fluorides at IKZ for their valuable support. S. Liang would like to thank the China Scholarship Council (CSC) for its financial support under Grant No. 201606020098.

REFERENCES

[1] J. Shi, D. Ahmed, X. Mao, S. S. Lin, A. Lawit, and T. J. Huang, Lab Chip **9**, 2890 (2009).
[2] V. Skowronek, R. W. Rambach, L. Schmid, K. Haase, and T. Franke, Anal. Chem. **85**, 9955 (2013).
[3] T. Zheng, C. Wang, D. Niu, W. Jiang, Y. Shi, L. Yin, B. Chen, H. Liu, and Y. Ding, RSC Adv. **4**, 46502 (2014).
[4] F. Guo, Z. Mao, Y. Chen, Z. Xie, J. P. Lata, P. Li, L. Ren, J. Liu, J. Yang, M. Dao, S. Suresh, and T. J. Huang, Proc. Natl. Acad. U. S. A. **113**, 1522 (2016).
[5] M. S. Brugger, S. Grundeen, A. Doyle, L. Theogarajan, A. Wixforth, and C. Westerhausen, Phys. Rev. E **98**, 012411 (2018).
[6] Y. Tang, D. Ao, W. Li, X. Zu, S. Li, and Y. Q. Fu, Sens. Actuators, B **254**, 1165 (2018).
[7] S. Okuda, T. Ono, Y. Kanai, T. Ikuta, M. Shimatani, S. Ogawa, K. Maehashi, K. Inoue, and K. Matsumoto, ACS Sens. **3**, 200 (2018).
[8] European Union, "Directive 2002/95/EC of the European Parliament and of the Council of 27 January 2003 on the restriction of the use of certain hazardous substance in electrical and electronic equipment," Off. J. Eur. Union L **37**, 19 (2003).
[9] R. Li, G. Li, W. Hong, P. I. Reyes, K. Tang, K. Yang, S. Wang, H. Ye, Y. Li, L. Zhang, K. Kisslinger, and Y. Lu, Smart Mater. Struct. **27**, 085025 (2018).
[10] L. Shao and K. P. Pipe, Appl. Phys. Lett. **106**, 023106 (2015).
[11] Z. Insepov, E. Emelin, O. Kononenko, D. V. Roshchupkin, K. B. Tnyshtykbayev, and K. A. Baigarin, Appl. Phys. Lett. **106**, 023505 (2015).
[12] S. Alzuaga, W. Daniau, R. Salut, T. Baron, S. Ballandras, and E. Defay, Appl. Phys. Lett. **105**, 062901 (2014).
[13] S. Liang, Y. Dai, L. von Helden, J. Schwarzkopf, and R. Wördenweber, Appl. Phys. Lett. **113**, 052901 (2018).
[14] R. Wördenweber, J. Schubert, T. Ehlig, and E. Hollmann, J. Appl. Phys. **113**, 164103 (2013).

[15]L. von Helden, M. Schmidbauer, S. Liang, M. Hanke, R. Wördenweber, and J. Schwarzkopf, Nanotechnology **29**, 415704 (2018).
[16]R. Wördenweber and Y. Dai, in *Strontium Titanate: Synthesis, Properties and Uses* (Nova Science Publishers, Inc., Materials Science and Technologies, New York, 2019), pp. 101–155.
[17]L. von Helden, L. Bogula, P.-E. Janolin, M. Hanke, T. Breuer, M. Schmidbauer, S. Ganschow, and J. Schwarzkopf, Appl. Phys. Lett. **114**, 232905 (2019).
[18]A. A. Bokov and Z.-G. Ye, Solid State Commun. **116**, 105 (2000).
[19]H. Vogel, Phys. Z. **22**, 645 (1921).
[20]G. S. Fulcher, J. Am. Ceram. Soc. **8**, 339 (1925).
[21]D. Viehland, S. J. Jang, L. E. Cross, and M. Wuttig, J. Appl. Phys. **68**, 2916 (1990).
[22]H. W. Jang, A. Kumar, S. Denev, M. D. Biegalski, P. Maksymovych, C. W. Bark, C. T. Nelson, C. M. Folkman, S. H. Baek, N. Balke, C. M. Brooks, D. A. Tenne, D. G. Schlom, L. Q. Chen, X. Q. Pan, S. V. Kalinin, V. Gopalan, and C. B. Eom, Phys. Rev. Lett. **104**, 197601 (2010).
[23]Q. J. Wang, C. Pflügl, W. F. Andress, D. Ham, and F. Capasso, J. Vac. Sci. Technol., B **26**, 1848 (2008).
[24]B. Cai, J. Schwarzkopf, E. Hollmann, M. Schmidbauer, M. O. Abdel-Hamed, and R. Wördenweber, J. Appl. Phys. **115**, 224103 (2014).
[25]X. Y. Du, Y. Q. Fu, S. C. Tan, J. K. Luo, A. J. Flewitt, W. I. Milne, D. S. Lee, N. M. Park, J. Park, Y. J. Choi, S. H. Kim, and S. Maeng, Appl. Phys. Lett. **93**, 094105 (2008).
[26]X. Y. Du, Y. Q. Fu, S. C. Tan, J. K. Luo, A. J. S. Maeng, S. H. Kim, Y. J. Choi, D. S. Lee, and N. M. Park, J. Phys.: Conf. Ser. **76**, 012035 (2007).
[27]T. Mino, S. Kuwajima, T. Suzuki, I. Kanno, H. Kotera, and K. Wasa, Jpn. J. Appl. Phys., Part 1 **46**, 6960 (2007).
[28]D. Damjanovic, Rep. Prog. Phys. **61**, 1267 (1998).
[29]R. C. Chang, S. Y. Chu, Y. P. Wong, Y. F. Lin, and C. S. Hong, Sens. Actuators, A **136**, 267 (2007).
[30]G. B. Kim, W. S. Chong, T. K. Kwon, K. Hohkawa, C. U. Hong, and N. G. Kim, Jpn. J. Appl. Phys., Part 1 **44**, 2868 (2005).